High-Temperature-Superconducting Weak Link Defined by the Ferroelectric Field Effect

L. Bégon-Lours, V. Rouco, A. Sander, J. Trastoy, R. Bernard,* E. Jacquet, K. Bouzehouane, S. Fusil, V. Garcia, A. Barthélémy, M. Bibes, J. Santamaría,† and J. E. Villegas‡

Unité Mixte de Physique, CNRS, Thales, Université Paris-Sud, Université Paris Saclay, 91767 Palaiseau, France

(Received 14 February 2017; published 12 June 2017)

In all-oxide ferroelectric (FE) superconductors (S), due to the low carrier concentration of oxides compared to transition metals, the FE interfacial polarization charges induce an accumulation (or depletion) of charge carriers in the S. This effect leads either to an enhancement or a depression of its critical temperature, depending on the FE polarization direction. Here, we exploit this effect at a local scale to define planar weak links in high-temperature-superconducting wires. These experiments are realized in $BiFeO_3$ (FE)/$YBa_2Cu_3O_{7-x}$ (S) bilayers in which the remnant FE domain structure is "written" by locally applying voltage pulses with a conductive-tip atomic force microscope. In this fashion, the FE domain pattern defines a spatial modulation of superconductivity. This characteristic allows us to "write" a device whose electrical transport shows different temperature regimes and magnetic-field-matching effects that are characteristic of Josephson coupled weak links. This behavior illustrates the potential of the ferroelectric approach for the realization of high-temperature-superconducting devices.

DOI: 10.1103/PhysRevApplied.7.064015

I. INTRODUCTION

The Josephson effect [1,2] results from the coupling of two superconductors (S) across an insulator (tunnel S-I-S junction) [3] or a weak link [4] (e.g., a normal metal in a proximity S-N-S junction) and constitutes the basis of a number of superconductor applications such as quantum-interference devices for magnetometry, digital electronics, signal processing, or medical imaging, among others [5].

Josephson applications were early realized using low-critical-temperature (T_C) superconductors. However, the advent of high-T_C superconductivity prompted efforts to create Josephson devices using high-T_C cuprates [6] capable of operating above liquid-nitrogen temperature. A versatile approach developed during the last decade exploits a nanoscale spatial modulation of T_C in a superconducting film [7,8]. This is accomplished by controllably introducing structural disorder (mostly oxygen interstitials and vacancies) on a local scale via masked ion irradiation or focused-ion beams. That type of disorder locally depresses T_C, which allows "patterning" the superconducting properties of the film [9,10]. Both S-N-S weak links [7,8] and S-I-S tunnel junctions [11] can be defined in this way. Besides yielding very reproducible Josephson characteristics [12], the key advantage of this approach is that the planar geometry allows for very large junction arrays [13], thus, opening the door to a variety of superconductor electronics applications [14].

In this paper, we investigate a different approach to define planar weak links in cuprate superconducting films. The idea is to create a nanoscale spatial modulation of T_C by electrostatic doping [15] through ferroelectric field effect [16–18]. This effect is achieved in ferroelectric (FE) superconductor (S) bilayers in which we combine a FE ($BiFeO_3$) whose polarization has a strong out-of-plane component [19] and a high-T_C superconductor ($YBa_2Cu_3O_{7-x}$). In this FE-S structure, if the FE polarization points away from the interface, holes are accumulated in the S to screen the negative polarization charges, which enhances T_C [red curve in Fig. 1(a)]. Conversely, if the FE points towards the interface, a hole depletion is induced, which leads to a depressed T_C [blue curve in Fig. 1(a)]. Switching between those two remnant states is achieved by momentarily applying a gate voltage to reverse the FE polarization [16–18]. Interestingly, this type of superconductivity modulation can be produced at a local scale, as sketched in Fig. 1(b), by artificially "writing" a FE domain pattern locally applying voltages with the conductive tip of an atomic force microscope (CT AFM) [20,21]. One of the prospects consists in "field-effect patterning" the superconducting condensate in a film to define circuits (such as Josephson arrays) that can be reversibly reconfigured via changes in the domain pattern [20,21]. With this perspective, here we explore a circuit defined by the FE domain structure shown in Fig. 1(b). The spatial modulation of the critical temperature created by this domain structure results in two superconductors

*Present address: Fonctions Optiques pour les Technologies de l'Information, UMR 6082, CNRS, INSA de Rennes, Rennes, France.

†Permanent address: GFMC, Departamento Fisica de Materiales, Facultad CC. Físicas, Universidad Complutense de Madrid, Madrid, Spain.

‡javier.villegas@cnrs-thales.fr

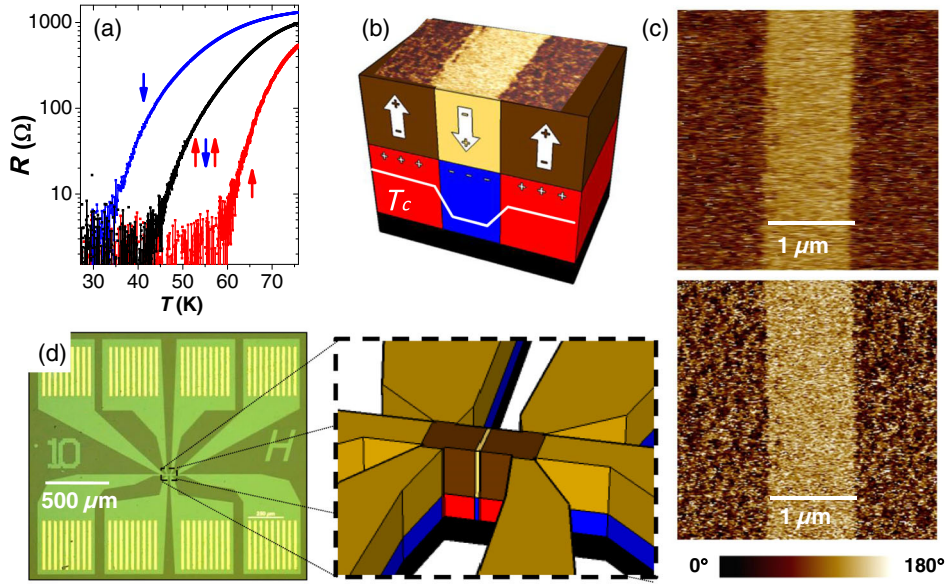

FIG. 1. (a) Subsequent resistance *vs* temperature measurements of a BFO/3-u.c. YBCO bridge fully polarized in the down state (blue curve), in the up state (red curve), and after the *S*-*S*'-*S* device is written (black curve). Bias current: 100 nA. (b) Schematic representation of the *S*-*S*'-*S* device. The upper layer represents the BFO with up- (brown) and down- (yellow) polarized domains. The lower layer represents the accumulated (red) and depleted (blue) YBCO regions. The field-effect-induced spatial modulation of the critical temperature T_C is shown. (c) Subsequent PFM phase images ferroelectric domains the day they are written (upper image) and after three weeks (lower image). The color scale shows the PFM phase in which 0° corresponds to upward polarization. (d) Optical microscope picture of the photolithographed multiprobe bridge and schematic representation of the area in which the ferroelectric structure is defined to create the *S*-*S*'-*S* junction.

connected by a superconducting region with a lower critical temperature T_C' (a *S*-*S*'-*S* junction). Using transport measurements, we find that within a given temperature range, the device behaves as a Josephson weak link and shows a nonmonotonic magnetoresistance related to flux quantization effects across *S*'. These results underscore the potential of the ferroelectric approach to tailor high-temperature-superconducting circuits.

II. EXPERIMENT

c-axis $YBa_2Cu_3O_{7-x}/BiFeO_3$ (YBCO/BFO) are grown using pulsed-laser deposition on [001] $SrTiO_3$ substrates that are previously treated (chemical etching in hydrofluoric acid followed by annealing at 1000 °C and in O_2) to obtain an atomically flat surface. Prior to YBCO deposition [either 3 or 4 unit cells (u.c.) for the samples studied here], a 3-u.c. buffer layer of $PrBa_2Cu_3O_{7-x}$ (PBCO, a wide-gap semiconductor isostructural to YBCO) is grown, which is known to enhance the superconducting properties of ultrathin YBCO. Note that ultrathin YBCO is required since the superconductor thickness must be comparable to the Thomas-Fermi screening length (approximately nanometers) [15] to maximize field-effect doping. Both PBCO and YBCO are grown at 690 °C in 0.35 mbar of pure O_2. Subsequently, an approximately 30-nm-thick BFO layer (with 5% substitution of Fe by Mn to reduce leakage currents [22]) is grown at 570 °C. The thickness of the different layers is adjusted from calibrated deposition rates. Further details on the growth and structural characterization of the films can be found elsewhere [19]. After growth, a multiprobe bridge [10 μm wide with voltage probes 40 μm afar; see Fig. 1(d)] for electrical measurements is patterned using photolithography and ion-beam etching. Contact pads to wire-bond YBCO through the BFO layer consist of a series of micrometric "trenches" etched across BFO and filled with evaporated Au. The ferroelectric domain structure is written by using a CT AFM and imaged via piezoresponse-force microscopy (PFM) as reported elsewhere [21]. We verify that the PFM images and, in particular, the size of the written ferroelectric domains, are stable over a time scale of a few weeks [see Fig. 1(c)]. After setting the desired ferroelectric state, samples are introduced in a closed-cycle refrigerator equipped with a 9-kG electromagnet and a rotatable sample holder to perform magnetotransport measurements.

III. RESULTS

Figure 1(a) shows the resistance vs temperature for a YBCO/BFO bilayer (YBCO thickness is 3 u.c.) in three different ferroelectric states: the red and blue curves, respectively, correspond to the cases in which the area in between the voltage probes is homogeneously polarized "up" and "down." The observed T_C shift is due to the change of the sheet carrier density Δn_{2D} in the YBCO film induced upon

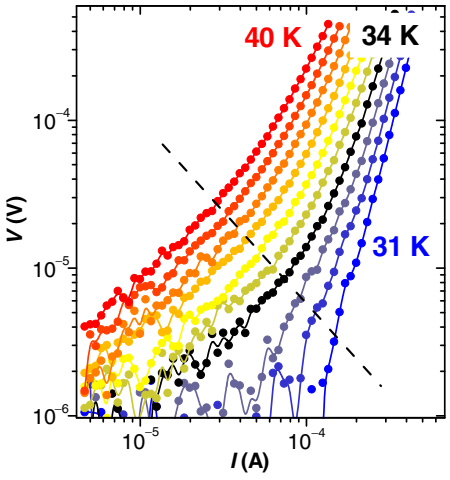

FIG. 2. Isothermal voltage-current characteristics of a BFO/3-u.c. YBCO device patterned with a *S*-*S*'-*S* structure (*S*' is 1 μm long) for temperatures between 40 and 31 K spaced by 1 K, under no applied magnetic field.

ferroelectric switching (Hall measurements in similar 3-u.c. samples allow us to estimate $\Delta n_{2D} < 2 \times 10^{14}$ cm^{-2}, which, as usual [21,23], is below approximately 8×10^{14} cm^{-2} expected from the nominal *c*-axis BFO ferroelectric polarization of approximately 70 μC cm^{-2} and suggests interfacial charge traps and/or incomplete ferroelectric switching). The black curve corresponds to a measurement after the *S*-*S*'-*S* structure shown in Figs. 1(b) and 1(c) is written. Note that the zero-resistance critical temperature for the *S*-*S*'-*S* device lies in between those for the up and down *FE* states (blue or red), which implies that the *S*' region is proximity coupled to the *S* regions.

Figure 2 shows $V(I)$ characteristics of the *S*-*S*'-*S* device in the 3-u.c. YBCO sample in zero applied magnetic field for a set of temperatures. Above approximately 34 K, we observe a nearly Ohmic tail at low currents and nonlinear behavior at higher currents. For lower temperatures, the Ohmic tail is no longer visible and yields to a steep $V(I)$ characteristic, with (seemingly) vanishing resistance in the low-current limit. Qualitatively, this behavior is reminiscent of the one observed in YBCO thin films as they undergo a second-order vortex glass transition [24]. However, the data depicted in Fig. 2 show significant quantitative differences from the theoretical expectations for that scenario. For instance, the crossover current I_{NL} above which nonlinear behavior is observed increases with decreasing temperature; this trend is marked with a dashed line in the figure. This is opposite to the theoretically expected behavior in the case of a vortex glass transition, where I_{NL} should decrease with decreasing temperature [25–27]. As we discuss further below, the different regimes observed in the $V(I)$ characteristics and the disagreement of the observed behavior with that of single YBCO films are connected to the weak-link behavior of the *S*-*S*'-*S* junction.

Magnetic field effects in the *S*-*S*'-*S* junction are investigated by measuring sets of $V(I)$ characteristics as a function of the applied magnetic field B for 31 K $< T <$ 40 K. B is applied perpendicular to the current and nearly parallel to the YBCO *a*-*b* planes (the misalignment is 5 ± 1 deg; the magnetotransport dependence on the field direction is discussed below). Figure 3 displays $V(I, B)$ for several temperatures (see legend) in color contour plots. Interpolated $I(B)$ curves for $V \sim 20$ μV and $V \sim 40$ μV is drawn in white as a guide to the eye. For all the temperatures, the $I(B)$ curves at constant voltage globally decreases with increasing magnetic field, yielding a nearly linear background. However, a nonmonotonic modulation is superposed to that background for the measurements shown in Figs. 3(b) and 3(c), which, respectively, correspond to 32 and 34 K. For these temperatures, the $I(B)$ curves show kinks (inflexion points) around $|B| \sim 4$ kG (white arrows). These features are most pronounced around 34–32 K and disappear for lower and higher temperatures. Note that the 34–32 K temperature range corresponds to the transition between the $V(I)$ curves showing an Ohmic tail and the $V(I)$ curves showing vanishing resistance in Fig. 2.

To further investigate the magnetic field modulation of dissipation and allow comparison between different samples and measurement conditions, we perform

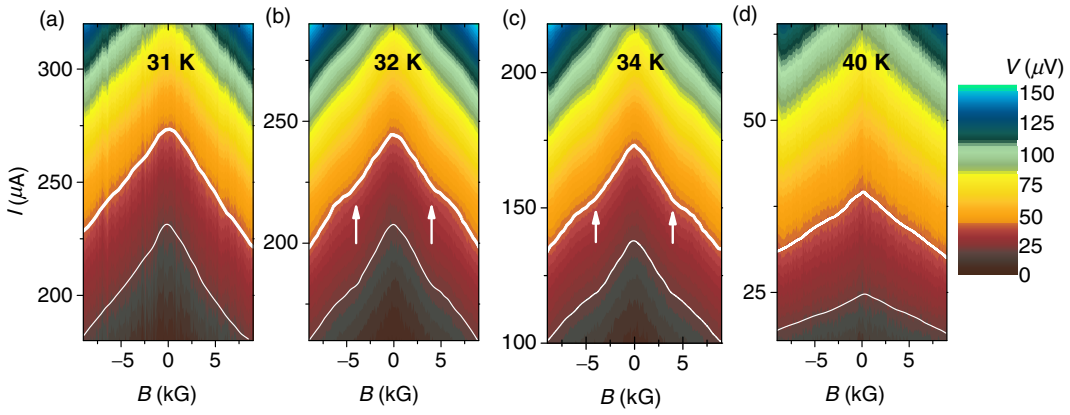

FIG. 3. Contour plot of the voltage-current characteristics for different applied magnetic fields ($\Delta B = 100$ G) for a BFO/3-u.c. YBCO bridge patterned with a 1-μm junction at different temperatures (see legends). The color code corresponds to the measured voltage (in V). Interpolated $I(B)$ curves for $V = 20$ μV and $V = 40$ μV is drawn in white as a guide to the eye.

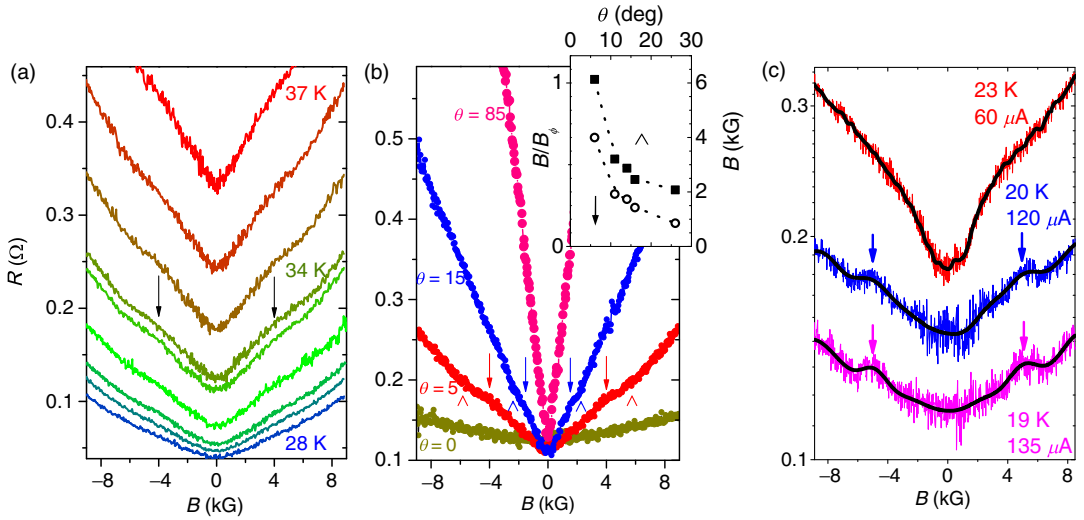

FIG. 4. Resistance *vs* applied magnetic field of a BFO/3-u.c. YBCO bridge patterned with a *S*-*S*'-*S* junction (*S*' is 1 μm long). In (a), the field is applied at an angle $\theta = 5° \pm 1°$ with respect to the YBCO *a*-*b* planes. The temperature ranges between 28 K (blue curve) and 37 K (red curve). In (b), the current and temperature are set at 120 μA and 34 K, and the angle θ with respect to the *a*-*b* planes is varied (see legend). Arrows (↓) and arrowheads (∧) point at the inflexion points for $\theta = 5° \pm 1°$ (red) and $\theta = 15° \pm 1°$ (blue). Inset: Characteristic magnetic fields at which inflexion points are observed as a function of θ. Squares and circles, respectively, correspond to the inflexion points marked with arrowheads (∧) and arrows (↓) in the main panel. The lines are a guide to the eye. The field is expressed in absolute units in the right *y*-axis scale, while in the left one, the field is normalized to the expected matching field B_ϕ (see text). (c) Resistance *vs* applied magnetic field for a BFO/4-u.c. YBCO bridge in which a *S*-*S*'-*S* structure is patterned (*S*' is 1 μm long). *B* is applied parallel to the YBCO *a*-*b* planes ($\theta = 0° \pm 1°$). The superposed black lines are obtained by smoothing (fast-Fourier-transform filter) the raw data (shown in color).

magnetoresistance measurements as a function of the temperature [Fig. 4(a)]. The resistance is calculated as $R = V/I$ from the voltage measured at constant current. Thus, the kinks seen in $I(B)$ curves (Fig. 3) appear inverted in $R(B)$ curves (marked with arrows in Fig. 4). One can see that the most pronounced effects appear in the temperature range of approximately 31–34 K.

In order to investigate the anisotropic effects, we perform magnetoresistance measurements as a function of the angle θ between *B* and the YBCO *a*-*b* planes, keeping the current perpendicular to *B*. Some of those measurements are shown in Fig. 4(b). Note that the kinks appear only in the angular range $0° < \theta < 30°$. As the magnetic field is rotated out of plane (i.e., on increasing θ), those features rapidly shift to lower fields and become weaker. Note also that the background magnetoresistance becomes much stronger with increasing θ, as expected from the very anisotropic nature of ultrathin YBCO [28]. The inset of Fig. 4(b) displays the characteristic fields at which the kinks appear, as a function of θ. Each kink is characterized by two fields which correspond to the two inflexion points, respectively, marked with a downward arrow (↓) and an upward arrowhead (∧) in the main panel curves. The trend observed in the inset of Fig. 4(b) suggests that the magnetoresistance kinks are not observed for $\theta = 0°$ because the characteristic fields grow out of the experimentally accessible window. Assuming that characteristic fields are related to a flux-matching phenomena, we seek to decrease it by increasing the sample section in parallel field. With this aim, we perform experiments in a YBCO/BFO bilayer with thicker YBCO—nominally 4 u.c.—in which a *S*-*S*'-*S* junction is written similar as in the 3-u.c. sample. For the 4-u.c. sample [see Fig. 4(c)], the magnetoresistance measurements in strictly parallel field ($\theta = 0°$) show matching effects within the experimental window. In particular, the resistance maxima (marked with downward arrows) are observed for $|B| \sim 5$ kG. Just as for the junction with 3-u.c.-thick YBCO, the nonmonotonic $R(B)$ is observed only within a very narrow (a few kelvins) range of temperatures. The characteristic matching field can be related to the section of the *S*' region via flux quantization arguments. In particular, using the thickness of the film $t \sim 4.4 \pm 1.1$ nm and the length of the *S*' barrier $l = 1 \pm 0.1$ μm, we can estimate the in-plane applied field that yields one flux quantum across the junction area as $B_\phi = \phi_0/tl = 4.7 \pm 1.3$ kG (with $\phi_0 = 2.07 \times 10^{-15}$ Wb), which is in good agreement with the experimental one $B \sim 5$ kG. If we perform an estimate for the 3-u.c. sample, a characteristic field $B_\phi = \phi_0/tl = 6 \pm 2$ kG is obtained. This value suggests that, for this sample, we cannot clearly see the magnetoresistance kink in strictly parallel field because it extends out of the experimental window.

IV. DISCUSSION

The observed behaviors can be understood if we consider that as the temperature is decreased, the *S*-*S*'-*S*

junction effectively behaves as (i) a decoupled *S*-*N*-*S* junction, (ii) a proximity-coupled *S*-*N*-*S* junction, or (iii) a continuous superconducting film. If we take as an example the measurements in the 3-u.c.-thick YBCO, the different regimes can be described as follows:

(i) At high temperatures (down to approximately 38 K in the example), the *S*-*S*'-*S* device behaves as decoupled *S*-*N*-*S* junction. The measured resistance corresponds to the addition of the resistances of *S* and *S*' in series. In this temperature range, *S* has not reached the zero-resistance state, and, since the ratio between the lengths of *S* and *S*' is approximately 40 μm/1 μm, the device resistance is essentially dominated by *S*. Thus, the resistance decreases with decreasing temperature and increases with increasing magnetic field. In this regime, due to the absence of coupling across *S*', $I(B)$ and $R(B)$ show no field-matching effects.

(ii) At intermediate temperatures ($\sim$32 K $< T <$ $\sim$38 K in the example), the *S* electrodes approach the zero-resistance state, and the system eventually starts behaving as a coupled *S*-*N*-*S* junction. In this regime, $I(B)$ and $R(B)$ show kinks related to flux quantization effects across *S*', which suggest Josephson coupling. In this scenario, we expect that the contribution of *S* and *S*' to the device resistance depends on the injected current and applied field. At low currents, i.e., below the critical current in *S*, the resistance is governed by the proximitized *S*' barrier. However, as the current and/or the magnetic field are increased, the contribution of the *S* electrodes increases. This current- and field-dependent weighting of the contribution in *S* and *S*' to the measured resistance explains the unusual temperature dependence of the crossover current I_{NL} (the nearly Ohmic tail corresponds to the response of *S*' above its critical current). It also explains the weakening of the field-matching effects with increasing current, which occurs as this exceeds the critical current in *S* thereby increasing its contribution to the measured resistance. Consistent with this scenario, the field-matching effects become stronger at temperatures below 34 K [see Figs. 3(a) and 4(a)]. This temperature corresponds to the temperature range in which $V(I)$ curves becomes nonlinear within the whole experimental window (see Fig. 2) due to the increase of the critical current in the proximitized *S*' barrier, thus, leading to stronger magnetic-field-modulation effects.

(iii) At the lowest temperatures (below 32 K in the example), the intrinsic critical temperature of the *S*' barrier is reached, and the device does not behave as a coupled *S*-*N*-*S* junction anymore but as a continuous *S*-*S*'-*S* superconducting film. Thus, $R(B)$ curves and $I(B)$ curves do not show field-matching effects related to Josephson coupling anymore.

In the above scenario, the rapid decrease of the matching field with increasing θ can be qualitatively understood considering that the junction area strongly depends on the magnetic field direction: while for the in-plane field component, the junction area is given by the length of *S*' times the superconductor thickness (as discussed previously), and for the out-of-plane component, the area is given by the length of *S*' times the width of the transport bridge (10 μm) and is, thus, much larger. This geometrical effect is further exacerbated by the fact that the in-plane and out-of-plane magnetic penetration lengths are very different due to the low film thickness [29]. Because of that, the effective junction area sharply increases as magnetic field is tilted out of the in-plane direction, from which we expect [30] the strong matching fields decrease, as observed in Fig. 4.

V. CONCLUSION

We define proximity-coupled *S*-*S*'-*S* weak links in high-temperature-superconducting wires by tailoring the domain structure of a ferroelectric overlayer. In particular, the local direction of the ferroelectric polarization is set so that the induced charge accumulation yields a local depression of superconductivity over a micron-size section of the wire. The field-effect-patterned devices show field-matching effects in the magnetoresistance, which are the signature of flux quantization effects characteristic of a proximity-coupled weak link. The micrometric width of the *S*' weak link sets a narrow temperature range over which the Josephson coupling between the *S* banks may occur. In particular, the temperature range is limited on the upper side by the required divergence of the coherence length of Andreev pairs in *S*' and on the lower side by the intrinsic critical temperature of *S*'. The present experiments illustrate the potential of the ferroelectric-field-effect approach for patterning high-temperature-superconducting oxide devices.

ACKNOWLEDGMENTS

This work is supported by the ERC Grants No. 64710 and No. 267579 and the French ANR Grant No. ANR-15-CE24-0008-01. L. B.-L. acknowledges a doctoral fellowship from DIM "OXYMORE" (Region Ile-de-France). J. S. thanks the CNRS "Institut de Physique" and Université Paris-Saclay (Programme Jean d'Alembert) for supporting his stay at Unité Mixte de Physique CNRS/Thales. J. T. thanks for the support from Fundación Barrié (Galicia, Spain). We thank J. Lesueur, N. Bergeal, and S. Bergeret for useful discussions.

[1] B. D. Josephson, Possible new effects in superconductive tunnelling, Phys. Lett. **1**, 251 (1962).

[2] B. D. Josephson, Supercurrents through barriers, Adv. Phys. **14**, 419 (1965).

[3] P. W. Anderson and J. M. Rowell, Probable Observation of the Josephson Superconducting Tunneling Effect, Phys. Rev. Lett. **10**, 230 (1963).

[4] K. K. Likharev, Superconducting weak links, Rev. Mod. Phys. **51**, 101 (1979).

[5] *100 Years of Superconductivity*, edited by H. Rogalla and P. H. Kes (Taylor & Francis, London, 2011).

[6] D. Koelle, R. Kleiner, F. Ludwig, E. Dantsker, and J. Clarke, High-transition-temperature superconducting quantum interference devices, Rev. Mod. Phys. **71**, 631 (1999).

[7] K. Chen, S. A. Cybart, and R. C. Dynes, Planar thin film $YBa_2Cu_3O_{7-\delta}$ Josephson junction pairs and arrays via nanolithography and ion damage, Appl. Phys. Lett. **85**, 2863 (2004).

[8] N. Bergeal, X. Grison, J. Lesueur, G. Faini, M. Aprili, and J. P. Contour, High-quality planar high-T_c Josephson junctions, Appl. Phys. Lett. **87**, 102502 (2005).

[9] J. Trastoy, M. Malnou, C. Ulysse, R. Bernard, N. Bergeal, G. Faini, J. Lesueur, J. Briatico, and J. E. Villegas, Freezing and thawing of artificial ice by thermal switching of geometric frustration in magnetic flux lattices, Nat. Nanotechnol. **9**, 710 (2014).

[10] J. Trastoy, C. Ulysse, R. Bernard, M. Malnou, N. Bergeal, J. Lesueur, J. Briatico,, and Javier E. Villegas, Tunable Flux-Matching Effects in High-T_c Superconductors with Nonuniform Pinning Arrays, Phys. Rev. Applied **4**, 054003 (2015).

[11] S. A. Cybart, E. Y. Cho, T. J. Wong, B. H. Wehlin, M. K. Ma, C. Huynh, and R. C. Dynes, Nano Josephson superconducting tunnel junctions in $YBa_2Cu_3O_{7-\delta}$ directly patterned with a focused helium ion beam, Nat. Nanotechnol. **10**, 598 (2015).

[12] M. Sirena, X. Fabrèges, N. Bergeal, J. Lesueur, G. Faini, R. Bernard, and J. Briatico, Improving the I_cR_n product and the reproducibility of high T_c Josephson junctions made by ion irradiation, Appl. Phys. Lett. **91**, 262508 (2007).

[13] S. A. Cybart, S. M. Anton, S. M. Wu, J. Clarke, and R. C. Dynes, Very Large Scale Integration of Nanopatterned $YBa_2Cu_3O_{7-\delta}$ Josephson Junctions in a Two-Dimensional Array, Nano Lett. **9**, 3581 (2009).

[14] S. Ouanani, J. Kermorvant, C. Ulysse, M. Malnou, Y. Lemaître, B. Marcilhac, C. Feuillet-Palma, N. Bergeal, D. Crété, and J. Lesueur, High-T_c superconducting quantum interference filters (SQIFs) made by ion irradiation, Supercond. Sci. Technol. **29**, 094002 (2016).

[15] J. Mannhart, High-T_c transistors, Supercond. Sci. Technol. **9**, 49 (1996).

[16] C. H. Ahn, S. Gariglio, P. Paruch, T. Tybell, L. Antognazza, and J. M. Triscone, Electrostatic modulation of superconductivity in ultrathin $GdBa_2Cu_3O_{7-x}$ films, Science **284**, 1152 (1999).

[17] C. H. Ahn, J.-M. Triscone, and J. Mannhart, Electric field effect in correlated oxide systems, Nature (London) **424**, 1015 (2003).

[18] C. H. Ahn, A. Bhattacharya, M. Di Ventra, J. N. Eckstein, C. Daniel Frisbie, M. E. Gershenson, A. M. Goldman, I. H. Inoue, J. Mannhart, A. J. Millis, A. F. Morpurgo, D. Natelson, and J. M. Triscone, Electrostatic modification of novel materials, Rev. Mod. Phys. **78**, 1185 (2006).

[19] A. Crassous, R. Bernard, S. Fusil, K. Bouzehouane, J. Briatico, M. Bibes, A. Barthélémy, and J. E. Villegas, $BiFeO_3/YBa_2Cu_3O_{7-\delta}$ heterostructures for strong ferroelectric modulation of superconductivity, J. Appl. Phys. **113**, 024910 (2013).

[20] K. S. Takahashi, M. Gabay, D. Jaccard, K. Shibuya, T. Ohnishi, M. Lippmaa, and J. M. Triscone, Local switching of two-dimensional superconductivity using the ferroelectric field effect, Nature (London) **441**, 195 (2006).

[21] A. Crassous, R. Bernard, S. Fusil, K. Bouzehouane, D. Le Bourdais, S. Enouz-Vedrenne, J. Briatico, M. Bibes, A. Barthélémy, and J. E. Villegas, Nanoscale Electrostatic Manipulation of Magnetic Flux Quanta in Ferroelectric/Superconductor $BiFeO_3/YBa_2Cu_3O_{7-\delta}$ Heterostructures, Phys. Rev. Lett. **107**, 247002 (2011).

[22] X. H. Zhu, H. Bea, M. Bibes, S. Fusil, K. Bouzehouane, E. Jacquet, A. Barthelemy, D. Lebeugle, M. Viret, and D. Colson, Thickness-dependent structural and electrical properties of multiferroic Mn-doped $BiFeO_3$ thin films grown epitaxially by pulsed laser deposition, Appl. Phys. Lett. **93**, 082902 (2008).

[23] H. Yamada, M. Marinova, P. Altuntas, A. Crassous, L. Bégon-Lours, S. Fusil, E. Jacquet, V. Garcia, K. Bouzehouane, A. Gloter, J. E. Villegas, A. Barthélémy, and M. Bibes, Ferroelectric control of a Mott insulator, Sci. Rep. **3**, 2834 (2013).

[24] J. Trastoy, V. Rouco, C. Ulysse, R. Bernard, A. Palau, T. Puig, G. Faini, J. Lesueur, J. Briatico, and J. E. Villegas, Unusual magneto-transport of $YBa_2Cu_3O_{7-\delta}$ films due to the interplay of anisotropy, random disorder and nanoscale periodic pinning, New J. Phys. **15**, 103022 (2013).

[25] M. P. Fisher, Vortex-Glass Superconductivity: A Possible New Phase in Bulk High-T_c Oxides, Phys. Rev. Lett. **62**, 1415 (1989).

[26] D. S. Fisher, M. P. A. Fisher, and D. A. Huse, Thermal fluctuations, quenched disorder, phase transitions, and transport in type-II superconductors, Phys. Rev. B **43**, 130 (1991).

[27] R. H. Koch, V. Foglietti, W. J. Gallagher, G. Koren, A. Gupta, and M. P. A. Fisher, Experimental Evidence for Vortex-Glass Superconductivity in Y-Ba-Cu-O, Phys. Rev. Lett. **63**, 1511 (1989).

[28] J. E. Villegas, Z. Sefrioui, M. Varela, E. M. Gonzalez, J. Santamaria, and J. L. Vicent, Interface barriers for flux motion in high-temperature superconducting superlattices, Phys. Rev. B **69**, 134505 (2004).

[29] J. Pearl, Current distribution in superconducting films carrying quantized fluxoids, Appl. Phys. Lett. **5**, 65 (1964).

[30] A. Barone and G. Paterno, *Physics and Applications of the Josephson Effect* (John Willey & Sons, Inc., New York, 1982).